Ceramics International 50 (2024) 37096–37110

Contents lists available at ScienceDirect

Ceramics International

journal homepage: www.elsevier.com/locate/ceramint

Variations of chemical, physical, mechanical properties, and biological and antimicrobial effectiveness of Ti alloys by coating with CaP doped with different amounts of Zn via micro-arc oxidation (MAO) technique

Senem Buyuksungur [a], Anca Constantina Parau [b], Mihaela Dinu [b], Iulian Pana [b], Catalin Vitelaru [b], Jürgen Schmidt [c], Tuğba Endoğan Tanir [d], Vasif Hasirci [a,e,f], Alina Vladescu (Dragomir) [b,g,*,1], Nesrin Hasirci [a,h,i,1,**]

[a] Middle East Technical University (METU), BIOMATEN, Center of Excellence in Biomaterials and Tissue Engineering, Ankara, 06800, Turkey
[b] National Institute of Research and Development for Optoelectronics - INOE 2000, 409 Atomistilor Str., 077125, Magurele, Romania
[c] INNOVENT e.V. Technologieentwicklung, Gruppenleiter Elektrochemie, Prüssingstraße 27b, Jena, 07745, Germany
[d] Middle East Technical University, Central Laboratory, Ankara, 06800, Turkey
[e] Acibadem Mehmet Ali Aydinlar University, Department of Medical Engineering, Istanbul, 34684, Turkey
[f] Acibadem Mehmet Ali Aydinlar University, Biomaterials Center, Istanbul, 34684, Turkey
[g] Research Center for Physical Materials Science and Composite Materials, National Research Tomsk Polytechnic University, Lenin Avenue 43, Tomsk, 634050, Russia
[h] Middle East Technical University, Department of Chemistry, Ankara, 06800, Turkey
[i] Near East University, Department of Bioengineering, 99138, Nicosia, TRNC, Mersin 10, Turkey

ARTICLE INFO

Handling Editor: Dr P. Vincenzini

ABSTRACT

Titanium alloys are preferred metals as implant materials due to their advantageous combination of low density and high biocompatibility. However, the augmentation of implant surfaces with calcium-based coatings becomes essential to regulate corrosion rates and enhance the osteoconductive properties of the implant material. In this study, titanium alloys, specifically Ti6Al4V, underwent a transformative process wherein they were coated with calcium phosphate (CaP) ceramics doped with zinc (Zn) via micro-arc oxidation (MAO) technique, using varying concentrations of Zn compound in the electrolyte solutions. The chemical and physical properties of the freshly prepared samples were analyzed, both initially and after culturing them with Saos-2 cells. Furthermore, the antimicrobial efficacy against *E. coli* was examined. The findings unveiled the remarkable efficiency of the MAO technique in forming an uniformly distributed coat on Ti6Al4V, thereby enhancing its mechanical resilience and biocompatibility, depending upon the preparation parameters employed. It was shown that Zn doped calcium coating is very efficient to regulate various parameters such as corrosion rate and mechanical strength, and an increase in Zn content exhibited a favorable impact on cell attachment and antimicrobial efficacy. Surface modification of metallic implants via MAO technique can be applied in the production of advanced implant materials.

1. Introduction

Medical devices such as orthopaedic and dental implants, artificial joints, cardiovascular devices as stents, which need mechanical strength and long-term stability in biological media are generally made of metals. It is required that these metals should be biocompatible with high corrosion resistance and antimicrobial activity if possible. In the last decades, research on titanium and titanium alloys progressed very fast and these alloys took the place of the stainless steel and cobalt-chromium implants due to their preferable stability, low density and high affinity towards osseointegration [1,2]. Osseointegration is the adhesion and proliferation of osteogenic bone cells on the implant

* Corresponding author. National Institute of Research and Development for Optoelectronics - INOE 2000, 409 Atomistilor Str., 077125, Magurele, Romania.
** Corresponding author. Middle East Technical University (METU), BIOMATEN, Center of Excellence in Biomaterials and Tissue Engineering, Ankara, 06800, Turkey.
E-mail addresses: alinava@inoe.ro (A. Vladescu (Dragomir)), nesrin.hasirci@neu.edu.tr, nhasirci@metu.edu.tr (N. Hasirci).
[1] Contributed equally as the corresponding authors

https://doi.org/10.1016/j.ceramint.2024.07.100
Received 30 April 2024; Received in revised form 28 June 2024; Accepted 8 July 2024
Available online 14 July 2024

surface which lead the bone growth on the metallic implant and strong adhesion of the implant to bone.

Although the expected life time is about ten years in dental and orthopaedic implants, lack of strong attachment between the implant and bone may cause loosening and problems, and a second operation may be needed to replace the implant. Therefore, osseointegration, strong attachment of the implant to the bone, is very important for the fixation and long-term functionality of the implant [3,4]. Since surface is the first part to come in contact with the natural bone, physical, chemical, mechanical properties and free energy of the surface of the implants play an important role in osteogenesis [5]. In order to have better bio-interaction with bone tissue, surface properties of the implant materials are improved via various surface modification techniques. There are physical methods as Plasma Immersion Ion Implantation and Deposition (PIII&D) and Plasma Spraying technique, or chemical methods as Electrolytic Deposition (ED) and Plasma Electrolytic Oxidation (PEO), or electrochemical technique as Micro-Arc Oxidation (MAO), or other techniques as Hydrothermal or Alkali heat treatment or Sol-gel for the modification of the implant surfaces [6].

Micro-arc oxidation (MAO) technique, which is conducted in electrolytic bath with application of energy, is generally used to form a ceramic oxide layer on metals to protect them from corrosion [7]. It is also known that the processing parameters of MAO, such as concentrations of electrolytes and acidity of the electrolyte solution, strength and time of the applied voltage influence the coat properties such as chemistry, crystal structure, thickness, roughness and porosity of the coatings [8–10]. It was reported that cell attachment and proliferation, and collagen deposition which leads to fast healing is more effective on rough surfaces compared to smooth ones [9]. On the other hand, if the fixation is not proper, this increases the bacterial attack and risk of infection at the host area [10]. Low friction and good wear resistance are also important for metals which are in contact with other surfaces and having sliding forces. For dental implants as well as hip or elbow joint implants, wear resistance is a crucial property. Lian et al. obtained a dense and thick double layer coat having inner titanium dioxide and outer silicon carbide (SiC) layers on the surface of Ti6Al4V by applying MAO technique to control wear resistance [11].

For medical implants, formation of calcium containing coatings gained importance to create bioactive coatings, since calcium is present in the natural bone and therefore implants having calcium on their surface enhance the attachment of the bone cells to the implant surface [12]. Qadir et al. gives a detailed review about calcium phosphate based composite coatings prepared by Micro-Arc Oxidation on implants made of commercially pure titanium (CP–Ti) and also biomedical grade Ti alloys [13]. The most commonly applied coating materials are the ones dicalcium phosphate dihydrate (DCPD), tricalcium phosphate (TCP) and hydroxyapatite (HAp), in general named as calcium phosphate (CaP) ceramics [14]. TCP is a fast degrading compound with Ca/P ratio of 1.5, meanwhile DCPD, also known as brushite, has Ca/P ratio of 1, and is also a precursor for HAp synthesis. HAp is the most commonly accepted and used calcium phosphate ceramic for medical devices since its structure is very similar to the natural bone. It is non-degradable and has Ca/P ratio of 1.67 similar to bone crystals [15].

Zinc is the one of the essential elements in the body and helps to growth and functions of organs, activates and regulates cellular signalling pathways and various physiological processes as well as bone growth and development [16]. Administration of zinc to rats led an increase in alkaline phosphatase activity related to DNA synthesis of bone tissue [17]. Due to the positive results obtained, scientists prepared different Zn added implant materials to examine their biocompatibility. Zhao et al. inserted high amounts of Zn ions into titanium dioxide nanotube arrays constructed on Ti implant materials by an electrochemical strategy, and reported controlled release performance of Zn [18]. Comaklı et al. examined the effects coats prepared by Ag2O, ZnO, NiO and nanocomposite films on commercially pure titanium applying sol-gel process. They reported increased hardness, tribological improved wear and corrosion resistance [19]. Kellesarian et al. collected the results of 10 *in vivo* studies in which Zn added Ti were implanted (5 in rabbits, 4 in rodents, 1 in goats), and reported that in all studies Zn containing implants enhanced new bone formation [20]. He et al. prepared Zn containing and Ti implant materials via plasma electrolytic oxidation (PEO) method, and inserted into 45 New Zealand white rabbits. Their observations were also supported the other with better and faster osseointegration and more bone deposition on Zn containing implant [21].

Application of an implant to aged people or the ones having osteoporosis is a problem since the regeneration of the bone is quite slow or not at all. Li et al. wanted to have an effective tooth restoration for osteoporotic bones of aged patients. They examined the integration of Ti rods inserted femoral metaphysis longitudinally into rats, where the rods were either coated by HAp or Zn-incorporated HAp. The samples coated with Zn-incorporated HAp needed higher push-out force proving better integration of the implants with bone [22]. Ito et al. synthesized zinc-containing tricalcium phosphate and hydroxyapatite ceramics by sintering, and reported that 1.2 wt% zinc significantly increased osteoblastic cell proliferation, and in 4 weeks almost 50 % higher bone formation in rabbits compared to the control group having no zinc [23]. Wang et al. investigated the behaviours of human gingival fibroblasts (HGFs), and cultured the cells with titanium implant materials loaded with magnesium and zinc by plasma immersed ion implantation technology. *In vitro* results demonstrated Mg ion-implanted samples exhibited better adhesion, and Zn ion-implanted samples demonstrated better proliferation [24].

It is well known that hospital-acquired infections are very common which negatively affect the health of patient [25]. Therefore, implant materials having antimicrobial surfaces preventing bacteria attachment are gaining importance. Addition of zinc into implant materials has great advantage besides enhancing bone growth, due to its antimicrobial effectiveness towards wide spectrum of bacteria without causing any toxicity to the host tissue [26,27]. Nistor et al. coated brass, copper and steel to enhance their corrosion resistance and antimicrobial affinity by nanoparticles of zinc oxide (ZnO) and silver (Ag), which were embedded in a silica matrix. They examined the effects of mono and bi-layer coats prepared on glass against *Bacillus cereus* strain and reported inhibitory effect of monolayer coatings having Ag or ZnO nanoparticles [28]. Varshney et al. prepared magnesium oxide (MgO) and ZnO nanoparticles by sol-gel method and combined them with hydroxyapatite in order to obtain artificial bone and bone implants. The results showed enhanced mechanical properties and antibacterial effectiveness against *B. subtilis*, *S. aureus*, and *E. coli* [29]. Mariappan also prepared Zn/Cu doped HAp nanocomposites by sol–gel technique and showed that the antibacterial activity against *K.pneumoniae*, *B. cereus* and *S. aureus* increased in a concentration dependent manner [30]. Meanwhile Predoi et al. showed that the antibacterial effect of Zn doped HAp depends on both the amount of Zn and stability [31]. In another study, Iqbal et al. coated Mg substrate with Zn doped hydroxyapatite−zeolite (ZnHA−Zeo) and polycaprolactone (PCL) composite and showed that the Zn addition improved the antibacterial activity against *E. coli* [32].

Although there are many published data about the positive effects of zinc containing coats on corrosion and microbial attacks, there is no one examining the effects of different amounts of Zn doped into the ceramic layer using the same technique. In this study, variations of chemical, physical, mechanical properties, and biological and antimicrobial effectiveness of different amounts of Zn doped CaP coating on Ti alloys by MAO technique were examined. The novelty of the study is to present data of a serial organization of Ti-alloys doped with different concentrations of Zn.

2. Materials and methods

2.1. Processing of titanium samples

Ti6Al4V alloys were coated with CaP doped with different amounts of Zn by MAO technique using solutions having various amounts of salts as described previously [33]. As Zn source, zinc acetate ($C_4H_6O_4Zn$) was added to the electrolyte solutions as 25, 50, 75 or 100 g/L (The compositions of the electrolytes used are listed in Supplement as Table S1).

Deposition of CaP and Zn on Ti alloys occurred by a pulsed bipolar current generator repeating rate of 1 ms, as described previously [34]. All samples prepared were cultured with osteosarcoma cell line (Saos-2 cells) and their physical properties, chemical compositions, and biological affinities were evaluated before and after the cell culture treatments.

2.2. Materials used for cell culture assays

RPMI 1640, Fetal Bovine Serum (FBS, Heat-Inactivated), Penicillin/Streptomycin solution, and Trypsin EDTA Solution B (contains 0.25 % Trypsin and 0.05 % EDTA) were products of Biological Industries (BI, Israel). Geneticin (G418) was purchased from Roche (Switzerland).

2.3. Characterization techniques

These studies can be divided into two groups as; 1) Chemical, physical, mechanical characterizations, and 2) Biological and antibacterial studies.

2.3.1. Chemical, physical, mechanical characterizations

EDS Analysis: EDS analysis of the freshly prepared coatings was achieved by an Energy-dispersive X-ray spectroscopy (EDS) using a XFlash 430 H detector (detection limit of 0.1 wt%) attached to a Quantax 70 system (Bruker). For each sample, three different zones were investigated.

Scanning Electron Microscopy (SEM) and X-ray Spectroscopy (EDS) Analysis: Topography and chemistry of the surfaces were analyzed before and after cell culture assays using SEM (QUANTA 400F Field Emission SEM, FEI, The Netherlands) and its EDS module. For each coated sample, three different zones were investigated.

Method for Calculation of Pore Size Distribution: Pore sizes of the CaP and CaP + Zn coated samples were determined from the SEM micrographs by measuring diameter of at least 50 pores per image using NIH ImageJ software (USA). Pore size distribution of the samples was calculated via frequency distribution analysis in GraphPad Prism 8.0.1 software (GraphPad Software Inc., La Jolla, USA) using the pore size measurements. Histograms represents relative frequency (%) vs. pore size (μm) were plotted using GraphPad Prism 8.0.1 software (GraphPad Software Inc., La Jolla, USA).

FTIR Analysis: The IR measurements were performed by a FTIR spectrometer (Jasco 6300) with an attached ATR unit (Pike Technologies) having Si/ZnSe crystal. The IR spectra of the samples were in the range of 4000-550 cm^{-1}. Prior to measurements, the ATR unit, detector and interferometer compartments were continuously purged by a constant flow of nitrogen gas. To ensure good spectral quality, the samples were further mounted on the Si/ZnSe crystal's surface using a high-pressure clamp. Single beam spectra of the background and sample were obtained at resolution of 4 cm^{-1} and 150 average scans. As cleaning solution for the crystals, isopropyl alcohol was used and the background spectrum was registered following each single IR measurement. For each coating, two different samples were investigated.

Scratch Tests: For the scratch test a diamond indenter (size of 200 μm) was used. Analyses were achieved by UMT-TriboLab platform (Bruker) having an acoustic sensor. The force from 0 to 50 N was put in application with a rate of 5 mm/min. This is in a good agreement with BS EN 1071–3:2005 standard which is defined for coatings having thickness of min. 2 μm. The adhesion was evaluated by identifying the critical load (Lc), where the failure of the coating occurs, being seen by direct microscopic observation as well as using the acoustic sensor (EN 1071–3/2005 standard). For each coating, three different samples were investigated.

Nanoindentation Tests: The nanomechanical tests were performed by using a Hysitron TI Premier indenter equipped with a Berkovich tip with a curvature radius of 100 nm and an included angle of 142.30. Several sources of uncertainty and error, including initial penetration depth, thermal drift, machine compliance and indenter area function were taken into consideration before nanoindentation measurements [35]. The calibration of the applied force was achieved on standard fused quartz specimen with H = 9.25 GPa ± 10 % and E = 69.6 GPa ± 10 %. The following two factors were taken into account in accordance with ISO 14577–1:2015 in order to prevent the impact of the Ti6Al4V on the resulting mechanical properties and the restrictions resulted by the geometrical shape of the Berkovich tip used in the experiements. As a result, the maximum indentation higher than 40 nm and the contact depths were less than 1/10 of the total coat thickness. By using a maximum indentation load of 1.5 mN, the load-displacement curves were used to determine the hardness (H) and reduced elastic modulus (Er). In terms of loading, holding, and unloading, the appropriate time intervals for a full indentation test were 7 s, 2 s, and 7 s, respectively. For nanoindentation tests on each sample, a total of at least 30 different locations were chosen at a distance of approximately 5 μm apart of each other.

***In Vitro* Electrochemical Investigation:** The corrosion resistance at the simulated body fluids (SBF) attack at 37 ± 0.4 °C was performed using VersaSTAT 3 Potentiostat, in accordance with the protocol related in ASTM standard G 59–97. The composition of SBF is given previously [36], and pH was kept at 7.2. The electrochemical cell consisted in calomel reference electrode, counter electrode (SCE, platinum sheet) and working electrode (WE–samples). The open circuit was monitored for 1 h after immersion in SBF. The Tafel tests was performed from −0.5 V vs. OCP to 1 V vs. SCE using a scan rate of 0.1667 mV/s. By Tafel extrapolation of the anodic and cathodic overpotentials at ±50 mV, corrosion current density (*i*corr) and corrosion potential (*E*i = 0) were obtained, according to the protocol given previously [37]. Polarization curve versus potential-current density graphs were used to find the polarization resistance (*R*p) at the point where *I* = 0 [37]. Morphologies of the sample surfaces after they went through the corrosion tests was evaluated by a Tabletop SEM (TM3000, Hitachi, Tokyo, Japan). For each coating, two different samples were investigated.

Wettability Analysis with Contact Angle and Surface Free Energy: A goniometer (One Attension, Biolin Scientific, Sweden) was used to determine the surface free energies (γ) of the samples. For this purpose, contact angles (θ) of two liquids with known surface tension values, such as distilled water (γwater: 72.04 mJ m^{-2}) and N,N-Dimethylformamide (DMF) (γDMF: 36.35 mJ m^{-2}) were used. Zisman plot in which 1-cosθ vs surface tension of the liquids were plotted, and the surface free energy (γ) of the solid samples were calculated from the graph using their measured contact angles as described previously [33]. For each coating, two different samples were investigated.

Surface Roughness Analysis: Surfaces of the samples were examined using surface profilometer (S Neox, Sensofar, Spain) to determine roughness values as "root mean squared height (Sq)" and "arithmetical mean height (Sa)" before and after cultured with Saos-2 cells. For each coated sample, three different zones were investigated.

2.3.2. In vitro cell culture tests

Indirect Cytotoxicity Assay: Cytotoxicity assays of the samples were assessed using extraction method in compliance with ISO 10993-5 standard following the procedure described in our previous study [33]. Briefly, samples were incubated in cell culture media to obtain extracts. Then, these obtained extracts were added on L929 cells and incubated for 24, 48 and 72 h in order to determine if there is any possible toxic

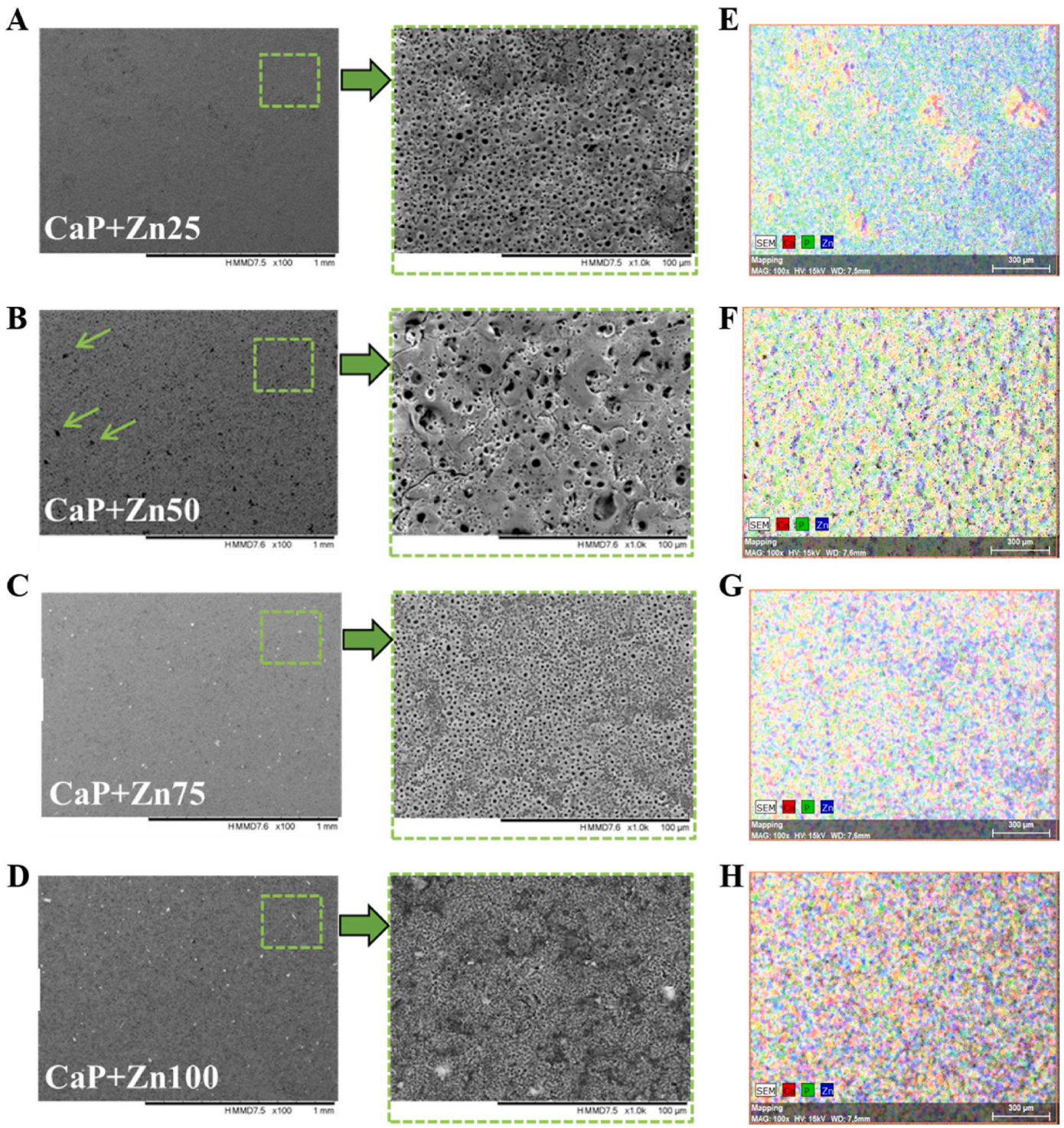

Fig. 1. SEM micrographs of CaP + Zn coatings on Ti alloy surfaces and EDS mapping of distribution of each element of the coating. A and E) CaP + Zn25; B and F) CaP + Zn50; C and G) CaP + Zn75; D and H) CaP + Zn100. (Scale bars: 1 mm for SEM images on left; 100 µm for SEM images in the middle; 300 µm for EDS mapping images on right).

effect of leachable molecules. Latex and ultra-high molecular weight polyethylene (UHMWPE) were used as negative and positive controls, respectively. Cytotoxicity was evaluated using the parameters of confluency, decrease in cell number, and change in the shape of the cells (Supplement).

Cell Viability and Cell-Material Interactions: Interaction of the material with cells was examined using Saos-2 cells. For this purpose, the cells ($5x10^4$ cells/sample) were seeded on the samples which were sterilized with ethanol prior to achieve the tests. Live/Dead Cell Viability Assay was achieved on days 2 and 7 using confocal laser scanning microscope (CLSM, LSM 800, Zeiss, Germany).

Antibacterial Tests: Samples before and after surface modifications were analyzed for the antibacterial efficiency of the coating materials against *Escherichia coli* (*E.coli*) as described previously [34]. Briefly, *E. coli* suspensions obtained from agar disks (0.5 McFarland turbidity) were added on the samples and incubated for 48 h. The attachment of

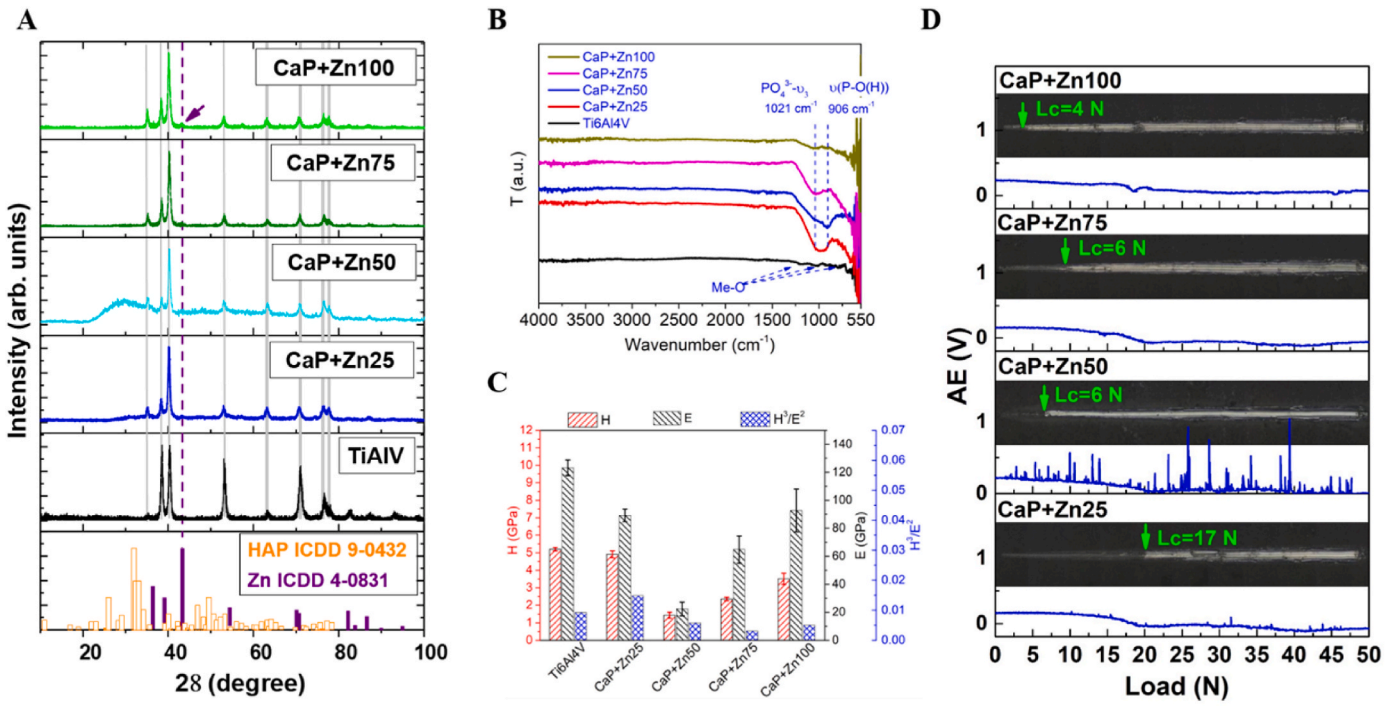

Fig. 2. A) XRD patterns of CaP + Zn coatings on Ti6Al4V surfaces. B) ATR-FTIR spectra of CaP + Zn coatings on Ti6Al4V alloys. C) The averaged values of hardness (H) and reduced modulus (Er) of CaP + Zn coatings on Ti6Al4V alloys, according to Oliver-Pharr formalism. D) Scratch test results of CaP + Zn coatings on Ti6Al4V alloys.

the bacteria was examined under SEM after fixation process with glutaraldehyde (2.5 %, v/v). *E.coli* on the SEM micrographs were pseudocolored by Adobe Photoshop software in order to obtain better visualization. NIH Image J program was used to determine the number of bacteria on the experimental samples (C_t) and the control group agar (C_0) per 225 μm^2 area. Antibacterial rates of the samples were determined using the following equation [38].

$$\text{Antibacterial Rate (\%)} = [(C_0 - C_t)/C_0] \times 100$$

Statistical Analysis: All experiments were performed as triplets and the data were evaluated using ANOVA or Tukey tests in GraphPad Prism 8.0.1 software (GraphPad Software Inc., La Jolla, USA. The results were evaluated as nonsignificant when p-values were higher 0.05, and highly significant when p-values were smaller than 0.01.

3. Results and discussion

3.1. Coatings: morphology and elemental composition

Morphology of the coatings were examined via SEM analyses, and the images obtained for CaP coatings having different Zn contents are presented in Fig. 1 A-D. Different magnifications of the same image can be observed for each sample, as following: an image showing the overall morphology on a larger area (x100) and a higher magnification image needed for in detail observation (x1000). As observed in the small magnification micrographs, all coatings are relatively uniform, except CaP + Zn50, where some defects are observed on the surface (indicated by arrows in Fig. 1B). At higher magnification, a porous structure is observed for all the coatings, however, higher visible pore sizes are characteristic to CaP + Zn50 morphology. For the rest of the samples, the pore sizes are decreasing as a function of Zn content, a higher concentration leads to a denser structure (Fig. 1D).

Elemental compositions were obtained as atomic concentrations of the constituent elements of the coatings (the elements of substrate (Ti, Al and V) were eliminated). As derived from EDS analysis, the amount of Zn increased by increasing of Zn content in the solution. The EDS mapping of the investigated surfaces indicates a homogeneous distribution of each element of the coating, showing that the coating covered well the whole surface of substrates (Fig. 1E–H). Percent amount of Ca decreased, while of P increased (Table S2). Thus, the ratio of Ca/P decreased, indicating the loss of the stoichiometry of apatite structure. According to the (Ca + Zn)/P ratio, the coatings with low Zn content exhibited an appropriate value to octacalcium phosphate (OCP) structure, which has excellent bone regenerative properties [39]. This result is positive because OCP structure is the most suitable to the composition of the natural bone [40]. Moreover, resorption rate of OCP is high, known as osteoinductive, and allows the addition of cations and anions for targeted functionalization [40–43]. By increasing the Zn content, the Ca/P decreased, indicating a trend towards to formation of calcium triphosphate structure (TCP with Ca/P = 1) and monocalcium phosphate (with Ca/P = 0.5). On the other hand, the decrease in the Zn content in the MAO layer of CaP + Zn100 indicates that, Zn can no longer be incorporated into the coating layer from a certain content with increasing the Zn concentration in the electrolyte. The surface morphology in the MAO process is highly dependent on the properties of the electrolyte system (pH value, conductivity, viscosity). Thus, the morphology was influenced by increasing the Zn concentration. In order to achieve a comparable coating thickness, the electrical parameters of the coating also had to be adjusted, resulting in a different morphology in CaP + Zn50 sample than for comparable variants.

According to the data obtained from pore size measurements (obtained from SEM micrographs by using GraphPad Software), CaP coated surfaces demonstrated the smaller pores (>3.0 μm) with a wider distribution compared to the Zn added ones – Fig. S2. Addition of Zn caused a change on pore sizes and pore distribution. The pores were smaller and homogeneously distributed for CaP + Zn25 and CaP + Zn75 samples with sizes less than 2.6 μm and 2.0 μm, respectively. The surfaces were quite smooth with smaller pores (>1.3 μm) for CaP + Zn100 samples. On the other hand, CaP + Zn50 samples demonstrated the most deviated pore size and distribution compared to the other samples, and had the largest pores (as large as 6.5 μm) having a non-homogeneous

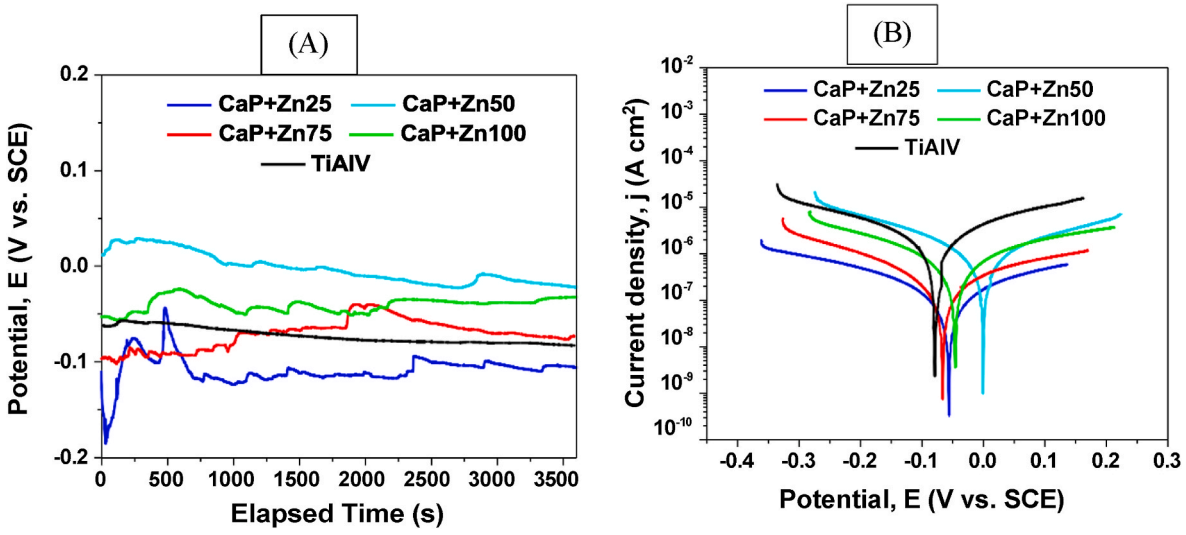

Fig. 3. (A) Open circuit potential vs time graphs and (B) Tafel plots of CaP + Zn coatings on titanium alloy surfaces.

Table 1
Corrosion parameters of the coatings.

Sample	Open circuit potential Eoc (mV)	Corrosion potential Ecorr (mV)	Corrosion current density icorr (μA/cm²)	Polarization resistance Rp (kΩ)
Ti6Al4V	−83.117	−77.054	3.183	23
CaP + Zn25	−106.12	−54.888	0. 394	335
CaP + Zn50	−22.389	1.207	1.864	44
CaP + Zn75	−73.302	−64.871	0.482	184
CaP + Zn100	−32.817	−44.558	1.762	68

distribution. The topography of the surfaces is also an important issue for the biocompatibility.

3.2. Phase composition and chemical bond

The diffraction patterns of zinc doped CaP based coatings are given in Fig. 2. The results show that Ti6Al4V has the specific diffraction peaks, as indicated. Note that CaP peaks (ICDD no. 09–0432) overlaps the diffraction lines attributed to Ti6Al4V substrate. According to the XRD analysis, no visible Zn associated maxima could be identified on the patterns of CaP with lower Zn concentration. However, a higher addition of this element led to the appearance of a small diffraction line in CaP + Zn100 spectra located at 43.25° (indicated by arrow). The identification was made based on ICDD no. 04–0831, where a hexagonal structure was revealed, fully textured by a single out-of-plane direction (101).

According to the ATR spectra of CaP + Zn coatings, there are two distinctive phosphate and hydroxyl functional groups in coat compositions (Fig. 2B). As a function of Zn amount increasing into CaP matrix, two main broad bands can be seen between 1200 and 900 cm^{-1}. In the case of CaP + Zn25 sample, one single broad band can be distinguished and attributed to asymmetric stretching mode of PO_4^{3-} ($\nu 3$) [44,45].

It should be noted that the chemical structure of CaP + Zn50 is starting to change by increasing Zn addition, another strong IR absorption band centered at 906 cm^{-1} being revealed in Fig. 2B. For instance, the weak shoulder corresponding to $\nu 3$ phosphate vibrational mode is still visible.

The peak at 906 cm^{-1} can be the vibration absorbance of P–OH stretching due to partially substitution of Ca^{2+} by Zn^{2+} ions. This stretching vibration of P–OH group is no longer visible for CaP + Zn75 and CaP + Zn100 samples due to poor crystallinity of coatings. The spectra showed the O–H stretching vibrations in the region located between 3500 and 4000 cm^{-1}, and incorporation of Zn^{2+} ions did not cause any effect on hydroxyl groups.

3.3. Mechanical properties of the coatings

The evaluation of the mechanical behavior of the coatings was carried out by measuring the hardness, elastic modulus, and adhesion between substrate and coating.

Hardness (H) and reduced modulus (Er) of CaP + Zn coatings: The hardness (H) and reduced Young modulus (Er) were determined by nanoindentation measurements using the Oliver-Pharr method [46,47], and the obtained results of H and Er are presented in Fig. 2C. The values of H and Er for the used Ti6Al4V substrate were 5.2 ± 0.1 GPa and 123.2 ± 5.5 GPa, respectively. The hardness of the Ti6Al4V alloy is still preserved after covering the substrate with the CaP + Zn25 coating which exhibited a hardness of 4.91 ± 0.2 GPa and a corresponding Er value of 89.2 ± 4.4 GPa. In this case, the value of Er is smaller by ~30 % as compared to the substrate. Although the results are comparable with other reported values of CaP coatings deposited on Ti6Al4V substrates [48], the rest of the coatings showed a suddenly drop (CaP + Zn50) followed by a linear increasing (CaP + Zn75 and CaP + Zn100) of the hardness and elastic modulus values. This tendency can be attributed at the same time for a different density and to a significant impact of indentation size on the nano-hardness behaviour of the coatings as a function of their obtained thicknesses by the electrochemical deposition route [49]. The resistance to plastic deformation can be evaluated by H^3/Er^{*2} ratio, the CaP + Zn25 coating being considered to be the most resistant among all investigated coatings according to Musil et al. [50].

Adhesion: Fig. 2D presents optical micrographs of scratch marks performed on the surface of each investigated coating and AE signal as a function of applied load. According to Kuptsov et al. an increase in AE signal can be related to the release of elastic energy generated by the propagation of semicircular cracks [51]. However, no cracks were identified along the associated scratches in the current study, the amplitude of the signal being low. The AE associated features present along the scratch mark performed on the CaP + Zn50 surface can be ascribed to a more pronounced porous morphology, as observed in SEM micrograph. By examination of the scratch morphology, the critical load was estimated for each system. As observed, the total delamination of CaP + Zn25 coating occurred at a normal load of 17 N, showing the highest adhesion to Ti6Al4V substrate among the investigated

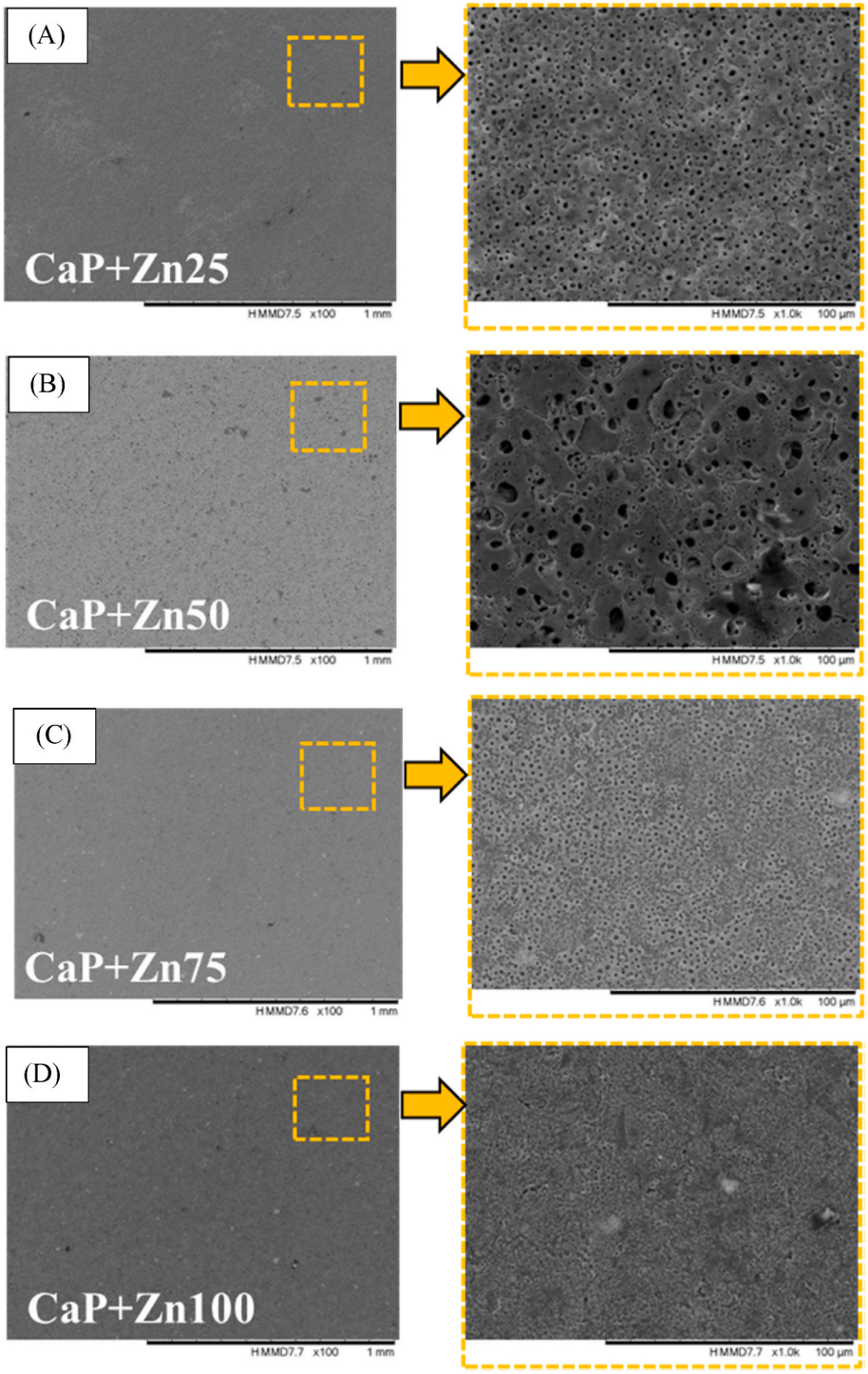

Fig. 4. SEM images of the CaP + Zn coatings obtained after corrosion tests.

specimens. In the case of the coatings with higher Zn content, the substrate material was exposed at lower loads, as following. Similar results of adhesion test were obtained for CaP + Zn50 and CaP + Zn75, indicating that further Zn increase did not induce significant changes and had no influence on the coating adhesion (Lc = 6 N). When the applied load reached 4 N, the detachment of CaP + Zn100 became visible. As shown in the literature, the addition of a high quantity of Zn leads to delamination [52], which is in accordance with the current results.

3.4. *In vitro* electrochemical tests

The corrosion results are further presented, the *in vitro* evaluation being considered a useful tool to give an insight on the sample's interaction with the biological environment. Fig. 3A presents the open circuit potential evolution (Eoc) in the absence of any polarization, values recorded during 1 h immersion in SBF testing medium. The Eoc values measured at the end of samples immersion (summarized in Table 1) represents an indication related to the material-electrolyte interface and the formation of passive layer with protective properties. According to *Presuel-Moreno* [53], the detrimental Cl^- anions which are present in all

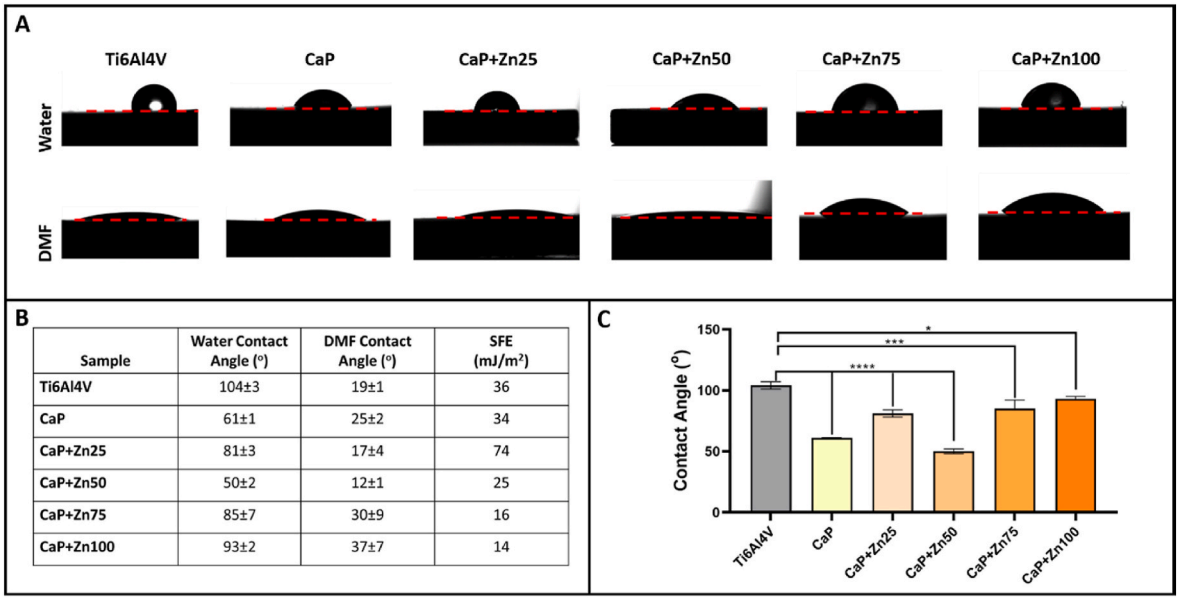

Sample	Water Contact Angle (°)	DMF Contact Angle (°)	SFE (mJ/m²)
Ti6Al4V	104±3	19±1	36
CaP	61±1	25±2	34
CaP+Zn25	81±3	17±4	74
CaP+Zn50	50±2	12±1	25
CaP+Zn75	85±7	30±9	16
CaP+Zn100	93±2	37±7	14

Fig. 5. Contact angle values of the unmodified and modified Ti6Al4V alloys. A) Contact angle images of the samples with water and DMF, B) Water and DMF contact angle values and calculated and SFE data of the samples, C) Graph showing the variation of the water contact angles of the unmodified and modified Ti6Al4V alloys.

chloride-containing solutions, can diffuse through the formed oxide films. Thus, a protective layer is highly dependent on the composition and can be seen as a barrier for the electrolyte ingress.

No decreasing tendency was observed for the investigated samples, only small fluctuations of potential over the tested period. CaP + Zn50 coating indicated the most electropositive value of Eoc among the investigated samples, indicating a tendency of protective film formation in time.

The Tafel plots of the CaP + Zn coatings (along with Ti6Al4V substrate) were presented in Fig. 3B and the extracted electrochemical parameters are shown in Table 1. One can note that charge transfer controlled reactions are highly influenced by surface morphology, and a porous structure as in the case of CaP + Zn50 allows the electrolyte ingress towards the substrate. Although the mentioned coating has the ability to form a more resistant surface oxide in the corrosive environment, indicated by the electropositive value of Ecorr (1.207 mV), the present pores behave as passing channels for the current flow, showing the highest icorr value measured (1.864 μA) and consequently, the lowest polarization resistance (44 kΩ). For the rest of the CaP coatings, there is a high dependence of electrochemical properties according to Zn addition: a higher concentration leads to an increase in corrosion current and a decrease of polarization resistance. The obtained results can be correlated with Zn depletion during immersion. The fact that Zn based ions can be released in the biological environment, and that can be considered in this case a more important weighing factor, by considering that zinc is one of the essential elements of the human body with confirmed beneficial effects on cell proliferation, viability and adhesion [54,55].

Surface morphology after corrosion tests: The surface morphology of the investigated Zn-doped CaP coatings after the corrosion assessment are shown in Fig. 4. Analyzing the micrographs, no visible evidence of a possible deterioration or the presence of corrosion products was observed. These findings suggest that the integrity of CaP coatings was maintained, promoting the chemical bond needed in the implant - bone tissue *in vivo* interaction.

3.5. Wettability and surface free energy

Protein absorption prior to cell adhesion is directly related with the wettability and surface free energy (SFE). Contact angles of unmodified and modified Ti6Al4V samples were determined using two different solvents, water and DMF, which have different surface energies of 72.04 mJ m^{-2} and 36.35 mJ m^{-2}, respectively. SFE of the samples with different coatings were calculated using Zisman plot (Fig. 5). Results showed that the unmodified Ti6Al4V sample were highly hydrophobic with water contact angle of 104±3°. Meanwhile the surface of the samples become more hydrophilic upon coating with CaP, CaP + Zn25 and CaP + Zn50. In the literature, it has been reported that the CaP coating on Ti alloys improve hydrophilicity [56,57]. In addition to that, there are studies showed that coating of solder alloy and MgCa1 alloy with Zn increased hydrophilicity [33,58]. However, as the concentration of Zn increased up to 75 and 100, the surface of the samples turned into hydrophobic again. SFE of the samples, on the other hand, increased upon coating CaP + Zn25, then as the concentration of Zn increased to 50, 75 and 100, SFE decreased again below that of uncoated Ti6Al4V sample.

3.6. Indirect cytotoxicity tests

In order to determine the cytotoxicity effect of the samples, indirect cytotoxicity tests were carried out. The tests were achieved according to ISO 10993/EN30993 MEM standards using L929 cells and extracts of the Ti6Al4V based samples as described previously [33]. Briefly, cell confluency, morphology, cell number and inhibition effect on the growth of the cells were analyzed after 24, 48 and 72 h of incubation. Evaluation of the cytotoxicity of the samples was performed according to the criteria and results are given in Supplement. In Fig. S1, results showed that the unmodified and modified Ti6Al4V samples demonstrated non-cytotoxic property in accordance with the studies in the literature [59,60].

3.7. Cell Viability and Cell-Material Interactions

Cell-material interaction tests were achieved with Saos-2 cells. The cells were seeded on unmodified and surface modified Ti6Al4V samples. The properties as adherence of the cells on the sample surfaces, their viability and the morphology were assessed on days 2 and 7 (Fig. 6). Cells seeded in tissue culture polystyrene (TCPS) were used as control. Live/Dead assay showed that after 2 days of culture there was a limited number of cells on unmodified Ti6Al4V. The adherence of the cells increased for CaP and CaP + Zn coated samples. Moreover, cell density

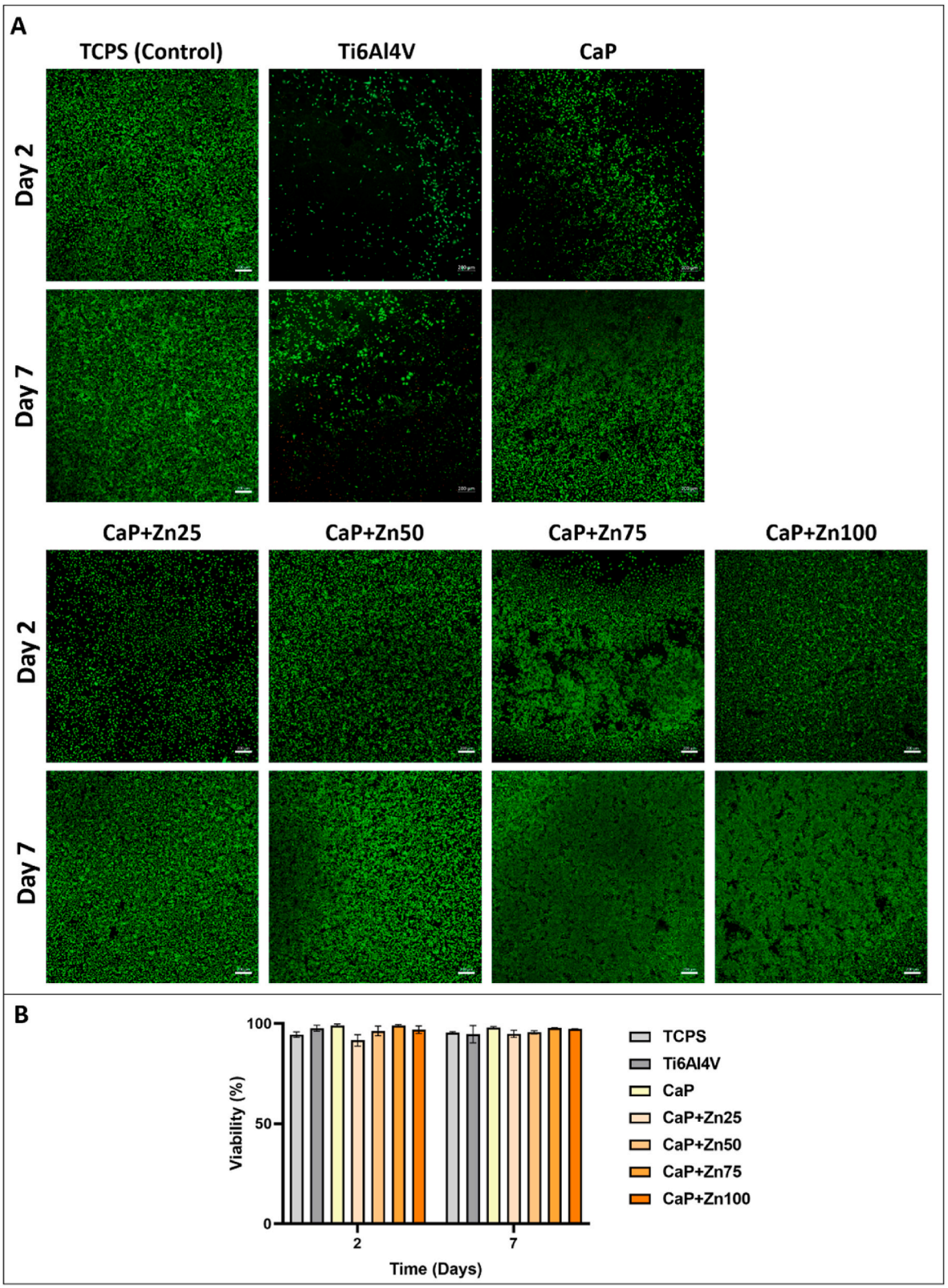

Fig. 6. Live-Dead Viability assessment of Saos-2 cells on Days 2 and 7. A) CLSM images of the cells on unmodified and surface modified Ti6Al4V samples co-stained with Calcein AM (Green, showing Live cells), and Ethidium Homodimer-1 (Red showing Dead cells). B) Graph showing Saos-2 cell viability (%) on the samples. TCPS was used as control. (Scale Bars: 100 μm). (For interpretation of the references to color in this figure legend, the reader is referred to the Web version of this article.)

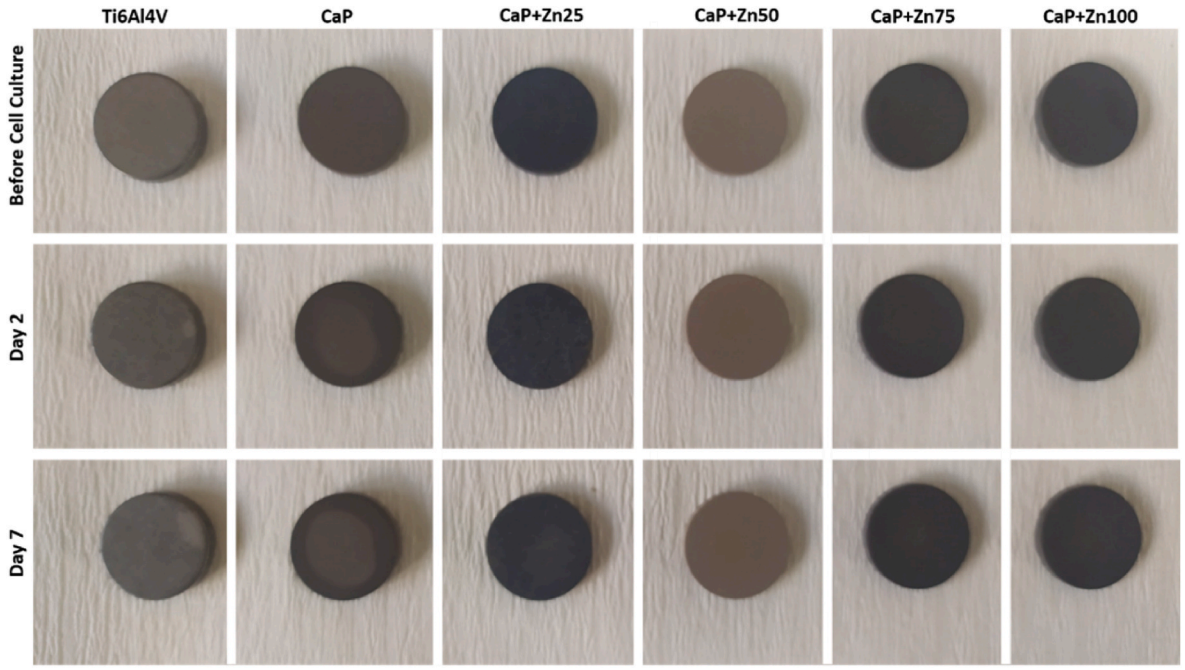

Fig. 7. The visual appearance of the Ti6Al4V based samples before and after 2 and 7 days of culturing with Saos-2 cells.

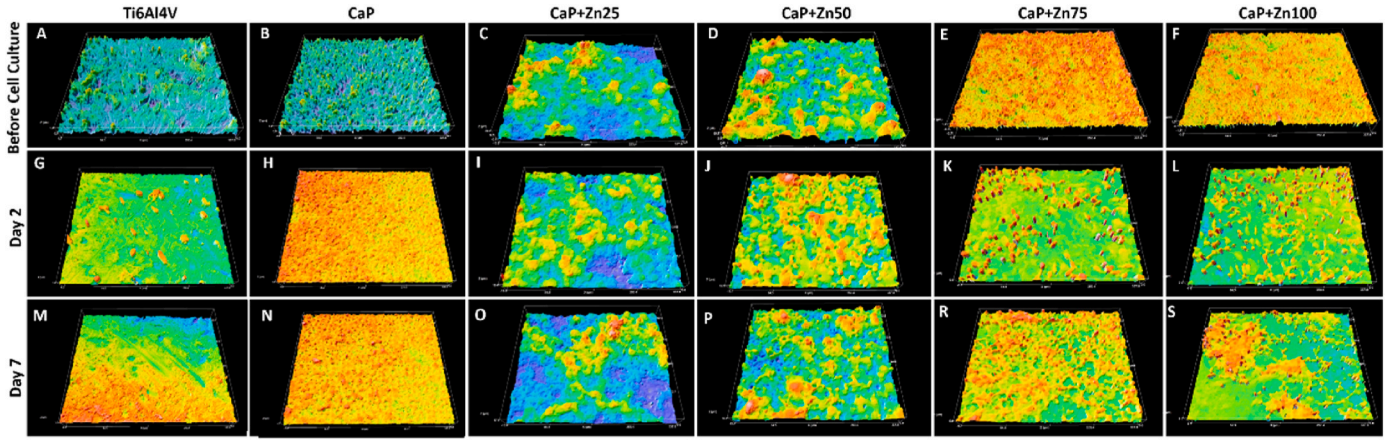

Fig. 8. Surface profilometer micrographs of unmodified and modified Ti6Al4V samples before (A, B, C, D, E, F) and after 2 (G, H, I, J, K, L) and 7 (M, N, O, P, R, S) days of Saos-2 cell culture.

on the CaP + Zn coated samples notably increased as the concentration of Zn increased. On the 7th day of culture, while cells proliferated well on both CaP and CaP + Zn modified samples, there is a slight increase in the number of the cells on unmodified Ti6Al4V. Results showed that the modification of the surfaces with CaP and CaP + Zn with the different concentrations of Zn improved cell adhesion and proliferation. On the other hand, the highest cell density on day 7 was observed for CaP + Zn75 and CaP + Zn100 coated samples. In the literature, Robatto et al. cultured MC3T3-E1 pre-osteoblast on hydroxyapatite (HA) and hydroxyapatite-zinc (Zn-HA) modified Ti6Al4V alloys and found that the cells adhered and spread well on the Zn-HA modified samples [61]. Viability of the cells was quantified using NIH Image J software through with confocal micrographs and found over 90 % for all of the groups even for unmodified Ti6Al4V samples which had the lowest cell number (Fig. 6B). Quantitative results of cell viability indicate that the samples do not exhibit any cytotoxicity.

3.8. Visual appearance of the materials

The visual appearance of the unmodified and coated samples was assessed before and after cell culture experiments (Fig. 7). The appearance of the coated samples was quite similar to the original ones with some slight color changes in between brownish and grey. Especially the CaP + Zn25 and CaP + Zn75 demonstrated the darkest color. It was interesting that CaP + Zn50 had the most brownish color compared to the others. Meanwhile, there was no visual change for the samples after 2 and 7 days of cell culture experiments which implies that the cell culture conditions did not affect the samples in a physical manner.

3.9. Surface Roughness Analysis

Surface roughness of all Ti6Al4V samples were examined with a surface profilometer. The tests were carried out for all samples before and after cell culturing with Saos-2 cells. Micrographs represents the surface topography and provide numerical values about the surface roughness (Fig. 8 and Table 2). In Table 2, Sq defines the standard

Table 2
Roughness of Ti6Al4V samples before and after cell culture assays (n = 3).

Sample	Property					
	Root mean square of heights Sq (μm)			Arithmetical mean deviation Sa (μm)		
	Before cell culture	After 2d cell culture	After 7d cell culture	Before cell culture	After 2d cell culture	After 7d cell culture
Ti6Al4V	0.48 ± 0.06	0.74 ± 0.06	1.05 ± 0.13	0.34 ± 0.04	0.55 ± 0.06	0.84 ± 0.14
CaP	0.86 ± 0.03	0.87 ± 0.07	1.15 ± 0.18	0.64 ± 0.02	0.70 ± 0.05	0.88 ± 0.14
CaP + Zn25	5.54 ± 0.39	4.50 ± 0.50	5.29 ± 0.46	4.65 ± 0.52	3.54 ± 0.39	4.11 ± 0.11
CaP + Zn50	4.24 ± 0.28	3.93 ± 0.17	4.52 ± 0.41	3.40 ± 0.21	3.13 ± 0.12	3.55 ± 0.32
CaP + Zn75	0.49 ± 0.02	1.12 ± 0.46	0.91 ± 0.70	0.38 ± 0.02	0.75 ± 0.28	0.73 ± 0.57
CaP + Zn100	0.39 ± 0.06	1.34 ± 0.54	1.58 ± 0.87	0.29 ± 0.04	0.97 ± 0.37	1.20 ± 0.65

deviation of height distribution, and Sa gives the mean difference in height from the arithmetical mean of the surface plane. Results showed that the surface topography changed upon coating with both CaP and CaP + Zn at different concentrations of Zn. Sq and Sa were significantly increased for the CaP + Zn25 ($p < 0000.1$) and CaP + Zn50 ($p < 0000.1$) modified samples compared to unmodified Ti6Al4V. Meanwhile, Sq and Sa values of CaP + Zn75 and CaP + Zn100 were similar with the uncoated samples before cell culture.

On the other hand, surface roughness of the uncoated Ti6Al4V, CaP, CaP + Zn75 and CaP + Zn100 modified samples affected during cell culture. Meanwhile it was observed that under the cell culture conditions surface roughness of the samples modified with CaP + Zn25 and CaP + Zn50 was not altered. Therefore, it can be concluded that the CaP + Zn25 and CaP + Zn50 modified samples showed a great stability in an aqueous environment.

3.10. Surface topography analysis

Surface topography of the samples was assessed by SEM analyses before and after 2 and 7 days of Saos-2 cell culture assays. Before cell culture, small scratches were observed for the surface of the unmodified Ti6Al4V samples (Fig. 9A–i and vii). Surface of the samples become porous upon coating with CaP and CaP + Zn (Fig. 9A–vii-xii). Meanwhile aggregation formation was also observed only for the CaP + Zn25 samples (Fig. 9A–ix). Saos-2 cell adherence with extended filopodia was observed for all of the sample groups. Nevertheless, adhered cell number was lowest for the unmodified Ti6Al4V sample compared to other modified groups on day 2 (Fig. 9B). However, on day 7 cell number increased for all of the groups (Fig. 9C). The cell behavior in terms of adherence and proliferation is parallel with the Live/Dead analysis results given in Fig. 6. On the other hand, appearance of the surfaces did not change after cell culture which implies that the surface modifications were stable under cell culture conditions.

3.11. Surface chemistry and elemental analysis

Elemental analysis of the coatings before and after cell culture studies were carried out by EDS (Table 3). Results showed that the atomic percent values (At, %) of carbon (C) and oxygen (O) increased after coating process for all of the sample because of oxidation. The presence of Ca and P on coated samples were observed for all of the modified samples before cell culture. However, as Zn concentration increased over 50, the atomic percentages of Ca and P detected in lesser extent. Meanwhile the atomic percentages of Ca and P did not change after cell culture, which implies that the stability of CaP coating. The presence of Zn was detected for Zn coated samples at different atomic percentages. After cell culture, while the Zn content did not undergo a significant change for CaP + Zn25 and CaP + Zn50, statistically important decrease was observed for the CaP + Zn75 and CaP + Zn100 samples.

3.12. Antimicrobial test results

In order to determine the antibacterial activity of the unmodified and coated Ti6Al4V, the samples were treated with gram-negative *E. coli*. The bacteria were added on samples and after 48 h, the surfaces were examined in terms of the bacterial shape, their distribution and colony forming capabilities on the surfaces (Fig. 10). Rod-like morphology was observed for *E. coli* on both unmodified and modified Ti6Al4V samples. Unmodified and CaP coated Ti6Al4V samples present microbial colonization in contrast to CaP + Zn modified samples. Number of *E. coli* on the micrographs were quantified per 225 μm^2 area and found as 24 ± 2, 21 ± 2, 2 ± 1, 2 ± 2, 20 ± 9, and 19 ± 7 for Ti6Al4V, CaP, CaP + Zn25, CaP + Zn50, CaP + Zn75, and CaP + Zn100 samples, respectively. Even though the amount is not as great as on agar, there is a certain number of bacteria on Ti6Al4V and CaP samples. Therefore, the antibacterial rate of Ti6Al4V and CaP samples actually represents the low adhesion of *E. coli* compared to the agar control. The significant antibacterial effect was observed for the CaP + Zn25 and CaP + Zn50 samples. Results indicate that the antibacterial effect of Zn is more noticeable for Zn25 and Zn50 samples (Fig. 10C). As the concentrations of Zn increased up to 75 and 100, the antibacterial effect of Zn could not be observed as much as desired. The antibacterial feature of Zn was observed in line with the studies previously reported in the literature [61–63].

Antibacterial rate was calculated using the agar group as a control. Since the agar surface is a natural growth environment for bacteria, it has enormously the highest number of bacteria attached on the surface (315 *E.coli*/225 μm^2) compared to the tested groups (which have attached bacteria in the range of 24 - 2 *E.coli*/225 μm^2). Eventhough the amount is not as high as on agar, there is a certain number of bacteria attached on Ti6Al4V and CaP coated samples. in the range of Therefore, the antibacterial rate of Ti6Al4V and CaP samples (92% and 93%, respectively) actually represents the low adhesion of *E.coli* compared to the agar control. The actual antibacterial effect was observed for the CaP + Zn25 and CaP + Zn50 samples with the antibacterial rate of 99 %.

4. Conclusions

In this study, Ti6Al4V alloys, which are the most commonly preferred implant materials, were coated with CaP and doped with different amounts of Zn by applying MAO technique. Results showed that surface topography changed upon coating, and homogeneous distribution of each element on the surfaces was obtained according to EDS mapping results. The amount of Zn in the coat did not increase parallel to the Zn content in the electrolyte solutions, most probably it cannot be doped more than a certain limiting value. Among all samples, CaP + Zn50 demonstrated differences compared to the others. These samples had defects on the surface, they had lowest hardness (H) and reduced modulus (Er) values, as well as the most electropositive value of Eoc indicating a tendency of protective film formation and the lowest polarization resistance. CaP coating and Zn doping on Ti alloys improved hydrophilicity of the alloys. The most hydrophilic ones CaP + Zn50 samples, and further increase in Zn concentration turned the samples to hydrophobic. Modification of Ti6Al4V surfaces enhanced cell adhesion and proliferation. After 7 days of culturing, surface roughness of CaP + Zn25 and

CaP + Zn50 samples was not changed, showing high stability of them in aqueous environment. These samples also had maximum efficacy against *E. coli*.

Cell proliferation and adhesion improved when the surfaces were modified with CaP and CaP + Zn. Furthermore, the viability of the cells was quantified as over 90 % for all of the groups, which indicates that

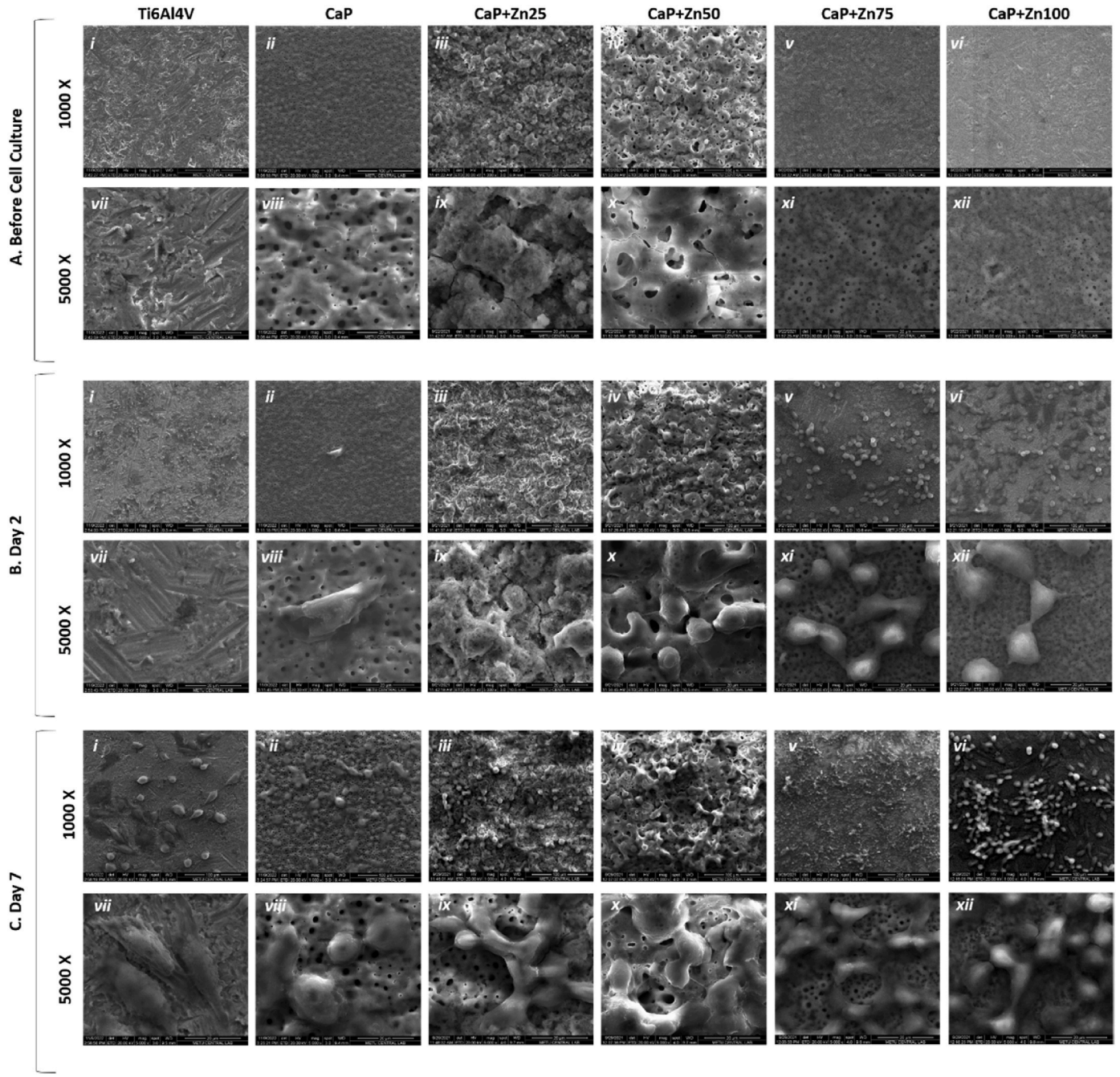

Fig. 9. SEM micrographs of unmodified and modified Ti6Al4V samples A) before, and B) after 2, and C) 7 days of Saos-2 cell culture. (Scale bars: 100 μm and 20 μm for 1000X and 5000X magnifications, respectively).

the samples do not exhibit any cytotoxicity. When these results were assessed along with the indirect cytotoxicity results, it can be concluded that the change in surface morphology depending on the Zn content did not lead to any cell toxicity.

As conclusion, MAO is an effective technique to coat titanium implant materials with CaP doped with Zn. Presence of zinc electrolytes in the solution can be absorbed on the surface to a certain value, and the coat effects almost all chemical, physical and mechanical properties, as well as cell affinity and microbial efficacy of Ti6Al4V alloys.

Funding

The present work was supported under a grant of ERA.Net" title = "http://ERA.Net">ERA.Net RUS-Plus project “CoatDegraBac” financed by the Romanian National Authority for Scientific Research, CNCS—UEFISCDI, project number COFUND-ERANET-RUS-PLUS-68/01.08.2018-CoatDegraBac (Romanian number), within PNCDI III, by The Scientific and Technological Research Council of Turkey (TUBITAK) (Project no. 9180035), and German Federal Ministry of Education and Research (Funding code 01DJ19004B).

CRediT authorship contribution statement

Senem Buyuksungur: Writing – original draft, Investigation. **Anca Constantina Parau:** Writing – review & editing, Investigation. **Mihaela Dinu:** Writing – review & editing, Investigation. **Iulian Pana:** Writing – review & editing, Investigation. **Catalin Vitelaru:** Writing – review & editing, Investigation. **Jürgen Schmidt:** Writing – review & editing,

Table 3
Atomic percent values of surface elemental compositions of Ti6Al4V based samples as determined with EDS module of SEM before and after culturing with Saos-2 cells.

	Elements on the surface (%)							
Samples	Ti	Al	V	Ca	P	Zn	C	O
Ti6Al4V								
Before cell culture	84.11 ± 0.37	13.22 ± 0.37	2.64 ± 0.04	N/A	N/A	N/A	N/A	N/A
After 2d culturing	85.31 ± 0.55	11.68 ± 0.32	3.00 ± 0.22	N/A	N/A	N/A	–	–
After 7d culturing	49.35 ± 1.97	5.93 ± 0.41	1.63 ± 0.13	N/A	N/A	N/A	–	–
CaP								
(Before cell culture	13.06 ± 0.32	1.37 ± 0.06	0.48 ± 0.06	6.66 ± 0.13	11.53 ± 0.14	N/A	N/A	N/A
After 2d culturing	14.08 ± 0.33	1.51 ± 0.14	0.56 ± 0.04	5.96 ± 0.09	11.28 ± 0.29	N/A	–	–
After 7d culturing)	14.10 ± 0.08	1.57 ± 0.21	0.38 ± 0.01	6.07 ± 0.16	11.44 ± 0.34	N/A	–	–
CaP + Zn25								
Before cell culture	5.34 ± 0.17	0.59 ± 0.09	0.32 ± 0.05	11.87 ± 0.48	11.15 ± 0.17	1.41 ± 0.10	23.88 ± 1.62	45.44 ± 0.92
After 2d culturing	6.53 ± 2.13	0.68 ± 0.27	0.29 ± 0.09	9.81 ± 0.63	10.00 ± 0.48	1.36 ± 0.16	26.55 ± 4.90	43.15 ± 2.04
After 7d culturing	8.93 ± 3.85	0.79 ± 0.37	0.33 ± 0.11	8.47 ± 0.58	8.71 ± 1.21	1.12 ± 0.11	28.53 ± 11.62	41.75 ± 8.35
CaP + Zn50								
Before cell culture	7.22 ± 0.25	0.95 ± 0.10	0.39 ± 0.05	3.17 ± 0.16	13.68 ± 0.39	3.70 ± 0.13	18.10 ± 1.15	51.95 ± 0.81
After 2d culturing	6.67 ± 1.85	0.85 ± 0.35	0.31 ± 0.09	2.96 ± 0.76	12.91 ± 3.80	3.54 ± 0.97	31.82 ± 5.23	50.31 ± 11.31
After 7d culturing	6.48 ± 0.50	0.81 ± 0.14	0.30 ± 0.08	2.98 ± 0.31	12.24 ± 0.99	3.46 ± 0.48	25.43 ± 5.52	47.24 ± 3.53
CaP + Zn75								
Before cell culture	36.53 ± 0.86	4.30 ± 0.09	1.58 ± 0.20	0.53 ± 0.06	3.40 ± 0.52	0.73 ± 0.02	0.00 ± 0.00	52.92 ± 0.54
After 2d culturing	26.91 ± 0.76	2.70 ± 0.12	0.95 ± 0.10	0.35 ± 0.06	2.46 ± 0.19	0.55 ± 0.09	24.29 ± 3.29	38.46 ± 1.55
After 7d culturing	29.23 ± 6.50	2.57 ± 0.78	0.93 ± 0.14	0.40 ± 0.08	2.69 ± 0.50	0.51 ± 0.07	24.82 ± 6.81	43.76 ± 9.84
CaP + Zn100								
Before cell culture	37.36 ± 0.77	4.32 ± 0.26	1.44 ± 0.15	0.38 ± 0.05	1.99 ± 0.06	0.41 ± 0.11	0.00 ± 0.00	54.10 ± 0.55
After 2d culturing	33.31 ± 8.71	3.63 ± 1.56	1.27 ± 0.37	0.38 ± 0.09	1.96 ± 0.40	0.00 ± 0.00	42.94 ± 9.98	46.16 ± 11.71
After 7d culturing	31.50 ± 6.58	3.61 ± 1.13	1.03 ± 0.27	0.30 ± 0.06	1.87 ±0 .46	0.23 ± 0.04	42.33 ± 10.85	45.68 ± 12.75

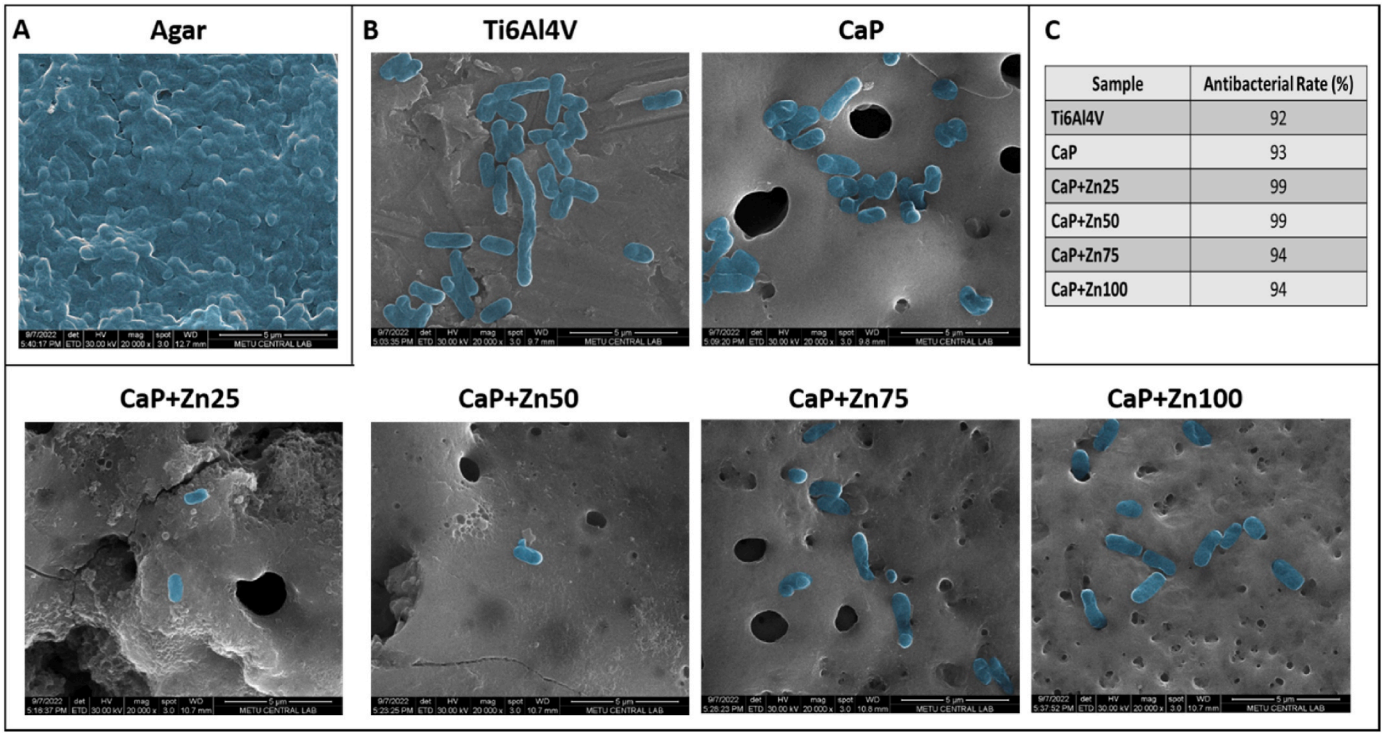

Fig. 10. SEM images of *E. coli* incubated for 48 h on A) Agar control, and B) Unmodified and modified Ti6Al4V samples. (Magnification: 20000X, Scale bars: 5 μm). C) Antibacterial rates calculated against *E. coli* (Bacteria on the images were pseudocolored with Adobe Photoshop software).

Supervision, Project administration, Methodology, Investigation, Funding acquisition, Formal analysis, Conceptualization. **Tuğba Endoğan Tanir:** Writing – review & editing, Formal analysis. **Vasif Hasirci:** Writing – review & editing, Supervision, Conceptualization. **Alina Vladescu (Dragomir):** Writing – review & editing, Writing – original draft, Validation, Supervision, Resources, Project administration, Investigation, Funding acquisition, Formal analysis, Conceptualization. **Nesrin Hasirci:** Writing – review & editing, Validation, Supervision, Resources, Project administration, Investigation, Funding acquisition, Formal analysis, Conceptualization.

Declaration of competing interest

The authors declare that they have no known competing financial interests or personal relationships that could have appeared to influence the work reported in this paper.

Acknowledgements

A.V. would like to thanks to Tomsk Polytechnic University within the framework of the Tomsk Polytechnic University-Competitiveness Enhancement Program grant. A.V. would like to mention that the experience gained during the development of the present experiments was well applied for the experiments developed during the project number ERANET-M-ISIDE-1, within PNCDI III, (project no. 171/2020) as well as by the Romanian Ministry of Research, Innovation and Digitalization through the National Research Development and Innovation Plan 2022–2027, Core Program, Project no: PN 23 05, contract no PN11N-03-01-2023. N.H. would like to thank BIOMATEN, METU Center of Excellence in Biomaterials and Tissue Engineering, for the use of the facilities. N.H. also thanks The Presidency of Strategy and Budget 08.11. KB(2016K121520) and TUBITAK for the financial support to BIOMATEN. We also thank P. Yilgor-Huri and S. Gokyer for carrying the indirect cytotoxicity tests. A.V. and N.H. thank ERA.Net" title = "http://ERA.Net">ERA.Net RUS-Plus project 'CoatDegraBac' for the support provided.

Appendix A. Supplementary data

Supplementary data to this article can be found online at https://doi.org/10.1016/j.ceramint.2024.07.100.

References

[1] Y.W. Cui, L. Wang, L.C. Zhang, Towards load-bearing biomedical titanium-based alloys: from essential requirements to future developments, Prog. Mater. Sci. 144 (2024) 101277, https://doi.org/10.1016/j.pmatsci.2024.101277.
[2] N. Hossain, M.A. Islam, M.S. Ahmed, M.A. Chowdhury, H. Mobarak, M. Rahman, H. Hossain, Advances and significances of titaniumin dental implant applications, Results in Chemistry 7 (2024) 101394, https://doi.org/10.1016/j.rechem.2024.101394.
[3] F. Rupp, L. Liang, J. Geis-Gerstorfer, L. Scheideler, F. Hüttig, Surface characteristics of dental implants: a review, Dent. Mater. 34 (2018) 40–57, https://doi.org/10.1016/j.dental.2017.09.007.
[4] F.A. Shah, P. Thomsen, A. Palmquist, A review of the impact of implant biomaterials on osteocytes, J. Dent. Res. 97 (2018) 977–986, https://doi.org/10.1177/0022034518778033.
[5] T. Hanawa, Titanium–tissue interface reaction and its control with surface treatment, Front. Bioeng. Biotechnol. 7 (2019) 170, https://doi.org/10.3389/fbioe.2019.00170.
[6] C. Gao, C. Li, C. Wang, Y. Qin, Z. Wang, F. Yang, H. Liu, F. Chang, J. Wang, Advances in the induction of osteogenesis by zinc surface modification based on titanium alloy substrates for medical implants, J. Alloys Compd. 726 (2017) 1072–1084, https://doi.org/10.1016/j.jallcom.2017.08.078.
[7] Y. Ge, B. Jiang, M. Liu, C. Wang, W. Shen, Preparation and characterization of the micro-arc oxidation composite coatings on magnesium alloys, J. Magnesium Alloys 2 (4) (2014) 309–316, https://doi.org/10.1016/j.jma.2014.11.006.
[8] A. Sobolev, I. Wolicki, A. Kossenko, M. Zinigrad, K. Borodianskiy, Coating Formation on Ti- 6Al-4V alloy by micro Arc Oxidation in molten salt, Materials 11 (9) (2018) 1611, https://doi.org/10.3390/ma11091611. PMID: 30181496. PMCID: PMC6163964.
[9] T. Albrektsson, A. Wennerberg, Oral implant surfaces: Part 1 – review focusing on topographic and chemical properties of different surfaces and in vivo responses to them, Int. J. Prosthodont. (IJP) 17 (5) (2004) 536–543. PMID: 15543910.
[10] M. Roy, A. Bandyopadhyay, S. Bose, Induction plasma sprayed nano hydroxyapatite coatings on titanium for orthopaedic and dental implants, Surf. Coat. Technol. 205 (8–9) (2011) 2785–2792, https://doi.org/10.1016/j.surfcoat.2010.10.042.
[11] Y. Lian, X. Dai, J. Zhang, Characterization of micro-arc oxidation coatings on Ti6Al4V with addition of SiC particle, Mater. Res. Express 7 (1) (2020) 016438, https://doi.org/10.1088/2053-1591/ab6c9a.
[12] C. Isikli, N. Hasirci, Surface and cell affinity properties of chitosan-gelatin-hydroxyapatite composite films, Key Eng. Mater. 493–494 (2011) 337–342. https://doi.org/10.4028/www.scientific.net/KEM.493-494.337.
[13] M. Qadir, Y. Li, K. Munir, C. Wen, Calcium phosphate-based composite coating by micro- arc oxidation (MAO) for biomedical application: a review, Crit. Rev. Solid State Mater. Sci. 43 (5) (2018) 392–416, https://doi.org/10.1080/10408436.2017.1358148.
[14] R. Narayanan, S.K. Seshadri, T.Y. Kwon, K.H. Kim, Calcium phosphate-based coatings on titanium and its alloys, J. Biomed. Mater. Res. B Appl. Biomater. 85 (1) (2008) 279–299, https://doi.org/10.1002/jbm.b.30932.
[15] S. Buyuksungur, T. Endogan-Tanir, A. Buyuksungur, E.I. Bektas, G. Torun-Kose, D. Yucel, T. Beyzadeoglu, E. Cetinkaya, C. Yenigun, E. Tönük, V. Hasirci, N. Hasirci, 3D printed poly(ε- caprolactone) scaffolds modified with hydroxyapatite and poly(propylene fumarate) and their effects on the healing of rabbit femur defects, 5, Biomater. Sci. 26 (10) (2017) 2144–2158, https://doi.org/10.1039/c7bm00514h. PMID: 28880313.
[16] B. Chen, P. Yu, W.N. Chan, F. Xie, Y. Zhang, L. Liang, K.T. Leung, K.W. Lo, J. Yu, G. M.K. Tse, W. Kang, K.F. To, Cellular zinc metabolism and zinc signaling: from biological functions to diseases and therapeutic targets, Signal Transduct. Targeted Ther. 9 (2024) 6, https://doi.org/10.1038/s41392-023-01679-y.
[17] M. Yamaguchi, R. Yamaguchi, Action of zinc on bone metabolism in rats: increases in alkaline phosphatase activity and DNA content, Biochem. Pharmacol. 35 (5) (1986) 773–777, https://doi.org/10.1016/0006-2952(86)90245-5.
[18] H. Zhao, W. Wang, F. Liu, Y. Kong, X. Chen, L. Wang, W. Ma, C. Liu, Y. Sang, X. Wang, S. Wang, H. Liu, Electrochemical insertion of zinc ions into self-organized titanium dioxide nanotube arrays to achieve strong osseointegration with titanium implants, Adv. Mater. Interfac. 9 (16) (2022) 2200312, https://doi.org/10.1002/admi.202200312.
[19] O. Çomakli, M. Yazici, T. Yetim, F. Yetim, A. Celik, Tribological and electrochemical behavior of Ag2O/ZnO/NiO nanocomposite coating on commercial pure titanium for biomedical applications, Ind. Lubric. Tribol. 71 (10) (2019) 1166–1176, https://doi.org/10.1108/ILT-11-2018-0414.
[20] S.V. Kellesarian, M. Yunker, R. Ramakrishnaiah, H. Malmstrom, T.V. Kellesarian, V.R. Malignaggi, F. Javed, Does incorporating zinc in titanium implant surfaces influence osseointegration? A systematic review, J. Prosthet. Dent 117 (1) (2017) 41–47, https://doi.org/10.1016/j.prosdent.2016.06.003.
[21] J. He, W. Feng, B.H. Zhao, W. Zhang, Z. Lin, In vivo effect of titanium implants with porous zinc-containing coatings prepared by plasma electrolytic oxidation method on osseointegration in rabbits, Int. J. Oral Maxillofac. Implants 33 (2) (2018), https://doi.org/10.11607/jomi.5764, 2018.
[22] X. Li, Y. Li, S. Peng, B. Ye, W. Lin, J. Hu, Effect of zinc ions on improving implant fixation in osteoporotic bone, Connect. Tissue Res. 54 (4–5) (2013) 290–296, https://doi.org/10.3109/03008207.2013.813495.
[23] A. Ito, H. Kawamura, M. Otsuka, M. Ikeuchi, H. Ohgushi, K. Ishikawa, N. Ichinose, Zinc-releasing calcium phosphate for stimulating bone formation, Mater. Sci. Eng. C 22 (1) (2002) 21–25, https://doi.org/10.1016/S0928-4931(02)00108-X.
[24] L. Wang, Q. Luo, X. Zhang, J. Qiu, S. Qian, X. Liu, Co-implantation of magnesium and zinc ions into titanium regulates the behaviors of human gingival fibroblasts, Bioact. Mater. 6 (1) (2021) 64–74, https://doi.org/10.1016/j.bioactmat.2020.07.012.
[25] J.A. Otter, S. Yezli, G.L. French, The role played by contaminated surfaces in the transmission of nosocomial pathogens, Infect. Control Hosp. Epidemiol. 32 (7) (2011) 687–699, https://doi.org/10.1086/660363.
[26] J. Sui, Y. Hou, M. Chen, Z. Zheng, X. Meng, L. Liu, S. Huo, S. Liu, H. Zhang, Nanomaterials for anti-infection in orthopedic implants: a review, Coatings 14 (3) (2024) 254, https://doi.org/10.3390/coatings14030254.
[27] L.K. Hakim, A. Yari, N. Nikparto, S.H. Mehbaran, S. Cheperli, A. Asadi, A. A. Darehdor, S. Nezaminia, D. Dortaj, Y. Nazari, M. Dehghan, P. Hojjat, M. Mohajeri, M.S.H. Jebelli, The current applications of nano and biomaterials in drug delivery of dental implant, BMC Oral Health 24 (2024) 126, https://doi.org/10.1186/s12903-024-03911-9.
[28] C.L. Nistor, C.I. Mihaescu, D. Bala, I.C. Gifu, C.M. Ninciuleanu, S.G. Burlacu, C. Petcu, M.G. Vladu, A. Ghebaur, L. Stroea, L.O. Cinteza, Novel hydrophobic nanostructured antibacterial coatings for metallic surface protection, Coatings 12 (2) (2022) 253, https://doi.org/10.3390/coatings12020253.
[29] S. Varshney, A. Nigam, A. Singh, S.K. Samanta, N. Mishra, R.P. Tewari, Antibacterial, structural, and mechanical properties of MgO/ZnO nanocomposites and its HA-based bio-ceramics; synthesized via physio-chemical route for biomedical applications, Mater. Technol. (2022) 1–14, https://doi.org/10.1080/10667857.2022.2043661.
[30] A. Mariappan, P. Pandi, K.B. Rani, K. Neyvasagam, Study of the photocatalytic and antibacterial effect of Zn and Cu doped hydroxyapatite, Inorg. Chem. Commun. 136 (2022) 109128, https://doi.org/10.1016/j.inoche.2021.109128.
[31] D. Predoi, S.L. Iconaru, M.V. Predoi, M. Motelica-Heino, R. Guegan, N. Buton, Evaluation of antibacterial activity of zinc-doped hydroxyapatite colloids and

dispersion stability using ultrasounds, Nanomaterials 9 (4) (2019) 515, https://doi.org/10.3390/nano9040515.
[32] N. Iqbal, S. Iqbal, T. Iqbal, H.R. Bakhsheshi-Rad, A. Alsakkaf, A. Kamil, M. R. Abdulkadir, M.H. Idris, H.B. Raghav, Zinc-doped hydroxyapatite-zeolite/polycaprolactone composites coating on magnesium substrate for enhancing in-vitro corrosion and antibacterial performance, Trans. Nonferrous Metals Soc. China 30 (1) (2020) 123–133, https://doi.org/10.1016/S1003-6326(19)65185-X.
[33] D.G. Tamay, S. Gokyer, J. Schmidt, A. Vladescu, P. Yilgor Huri, V. Hasirci, N. Hasirci, Corrosion resistance and cytocompatibility of magnesium–calcium alloys modified with zinc-or gallium-doped calcium phosphate coatings, ACS Appl. Mater. Interfaces 14 (1) (2021) 104–122, https://doi.org/10.1021/acsami.1c16307.
[34] J. Schmidt, I. Pana, A. Bystrova, M. Dinu, Y. Dekhtyar, C. Vitelaru, M. Gorohovs, I. M. Marinescu, P.Y. Huri, D.G. Tamay, G.A. Juravlea, S. Buyuksungur, A.C. Parau, V. Hasirci, N. Hasirci, A. Vladescu, Zn doped CaP coatings used for controlling the degradation rate of MgCa1 alloy: in vitro anticorrosive properties, sterilization and bacteria-/cell-material interactions, Colloids Surf. B Biointerfaces 113087 (2022), https://doi.org/10.1016/j.colsurfb.2022.113087-.
[35] J. Menčík, Uncertainties and errors in nanoindentation, Nanoindent. Mater. Sci. 54 (2012) 53–86, https://doi.org/10.5772/50002.
[36] D.M. Vranceanu, A.C. Parau, C.M. Cotrut, A.E. Kiss, L.R. Constantin, V. Braic, A. Vladescu, In vitro evaluation of Ag doped hydroxyapatite coatings in acellular media, Ceram. Int. 45 (2019) 11050–11061, https://doi.org/10.1016/j.ceramint.2019.02.191.
[37] P.F. Gostin, A. Gebert, L. Schultz, Comparison of the corrosion of bulk amorphous steel with conventional steel, Corrosion Sci. 52 (2010) 273–281, https://doi.org/10.1016/j.corsci.2009.09.016.
[38] M. Chu, H. Gao, S. Liu, L. Wang, Y. Jia, M. Gao, M. Van, C. Xu, L. Ren, Functionalization of composite bacterial cellulose with C 60 nanoparticles for wound dressing and cancer therapy, RSC Adv. 8 (33) (2018) 18197–18203, https://doi.org/10.1039/C8RA03965H.
[39] Y. Shiwaku, O. Suzuki, Octacalcium phosphate effects on the systemic and local factors that regulate bone-cell activity, in: Octacalcium Phosphate Biomaterials, Woodhead Publishing, 2020, pp. 17–36, https://doi.org/10.1016/B978-0-08-102511-6.00002-9.
[40] P. Habibovic, K. de Groot, Osteoinductive biomaterials—properties and relevance in bone repair, J. Tissue Eng. Regen. Med. 1 (2007) 25–32, https://doi.org/10.1002/term.5.
[41] R.M. Shelton, Y. Liu, P.R. Cooper, U. Gbureck, M.J. German, J.E. Barralet, Bone marrow cell gene expression and tissue construct assembly using octacalcium phosphate microscaffolds, Biomaterials 27 (2006) 2874–2881, https://doi.org/10.1016/j.biomaterials.2005.12.031.
[42] E.D. Deeks, S. Dhillon, Strontium ranelate: a review of its use in the treatment of postmenopausal osteoporosis, Drugs 70 (2010) 733–759, https://doi.org/10.2165/10481900-000000000-00000.
[43] A.S. Posner, F. Betts, Synthetic amorphous calcium-phosphate and its Relation to bone-mineral structure, Acc. Chem. Res. 8 (1975) 273–281, https://doi.org/10.1021/ar50092a003.
[44] F. Ren, Y. Ding, Y. Leng, Infrared spectroscopic characterization of carbonated apatite: a combined experimental and computational study, J. Biomed. Mater. Res. 102 (2) (2014) 496–505, https://doi.org/10.1002/jbm.a.34720.
[45] I. Rehman, W.J.J. Bonfield, Characterization of hydroxyapatite and carbonated apatite by photo acoustic FTIR spectroscopy, J. Mater. Sci. Mater. Med. 8 (1) (1997) 1–4, https://doi.org/10.1023/a:1018570213546.
[46] W.C. Oliver, G.M. Pharr, An improved technique for determining hardness and elastic modulus using load and displacement sensing indentation experiments, J. Mater. Res. 7 (6) (1992) 1564–1583, https://doi.org/10.1557/JMR.1992.1564.
[47] W.C. Oliver, G.M. Pharr, Measurement of hardness and elastic modulus by instrumented indentation: advances in understanding and refinements to methodology, J. Mater. Res. 19 (1) (2004) 3–20, https://doi.org/10.1557/jmr.2004.19.1.3.
[48] K.A. Khor, H. Li, P. Cheang, Characterization of the bone-like apatite precipitated on high velocity oxy-fuel (HVOF) sprayed calcium phosphate deposits, Biomaterials 24 (2003) 769–775, https://doi.org/10.1016/S0142-9612(02)00413-1.
[49] A. Dey, A.K. Mukhopadhyay, S. Gangadharan, M.K. Sinha, D. Basu, N. R. Bandyopadhyay, Nanoindentation study of microplasma sprayed hydroxyapatite coating, Ceram. Int. 35 (6) (2009) 2295–2304, https://doi.org/10.1016/j.ceramint.2009.01.002.
[50] J. Musil, P. Novák, R. Čerstvý, Z. Soukup, Tribological and mechanical properties of nanocrystalline-TiC/a-C nanocomposite thin films, J. Vac. Sci. Technol. A: Vacuum, Surfaces, and Films 28 (2) (2010) 244–249, https://doi.org/10.1116/1.3294717.
[51] K.A. Kuptsov, P.V. Kiryukhantsev-Korneev, A.N. Sheveyko, D.V. Shtansky, Comparative study of electrochemical and impact wear behavior of TiCN, TiSiCN, TiCrSiCN, and TiAlSiCN coatings, Surf. Coating. Technol. 216 (2013) 273–281, https://doi.org/10.1016/j.surfcoat.2012.11.058.
[52] D.M. Vranceanu, E. Ungureanu, I.C. Ionescu, A.C. Parau, A.E. Kiss, A. Vladescu, C. M. Cotrut, Electrochemical surface biofunctionalization of titanium through growth of TiO2 nanotubes and deposition of Zn doped hydroxyapatite, Coatings 12 (1) (2022) 69, https://doi.org/10.3390/coatings12010069.
[53] F. Presuel-Moreno, M.A. Jakab, N. Tailleart, M. Goldman, J.R. Scully, Corrosion-resistant metallic coatings, Mater. Today 11 (10) (2008) 14–23, https://doi.org/10.1016/S1369-7021(08)70203-7.
[54] H. Tapiero, K.D. Tew, Trace elements in human physiology and pathology: zinc and metallothioneins, Biomed. Pharmacother. 57 (9) (2003) 399–411, https://doi.org/10.1016/S0753-3322(03)00081-7.
[55] H. Begam, B. Kundu, A. Chanda, S.K. Nandi, MG63 osteoblast cell response on Zn doped hydroxyapatite (HAp) with various surface features, Ceram. Int. 43 (4) (2017) 3752–3760, https://doi.org/10.1016/j.ceramint.2016.12.010.
[56] S. Su, W. Chen, M. Zheng, G. Lu, W. Tang, H. Huang, D. Qu, Facile fabrication of 3D- printed porous Ti6Al4V scaffolds with a Sr-CaP coating for bone regeneration, ACS Omega 7 (10) (2022) 8391–8402, https://doi.org/10.1021/acsomega.1c05908.
[57] C. Zhang, G. Duan, J. Li, D. Xiao, F. Shi, K. Duan, T. Guo, X. Fan, J. Weng, Hydrothermal growth of biomimetic calcium phosphate network structure on titanium surface for biomedical application, Ceram. Int. 49 (11) (2023) 16652–16660, https://doi.org/10.1016/j.ceramint.2023.02.026.
[58] M.I.I. Ramli, M.A.A.M. Salleh, N.A. Saleh, S.F.M. Amli, Wettability and thermal properties of Sn-0.7 Cu-0.05 Ni-xZn solder alloy, IOP Conf. Ser. Mater. Sci. Eng. 701 (1) (2019) 012024, https://doi.org/10.1088/1757-899X/701/1/012024.
[59] A. Lerebours, P. Vigneron, S. Bouvier, A. Rassineux, M. Bigerelle, C. Egles, Additive manufacturing process creates local surface roughness modifications leading to variation in cell adhesion on multifaceted TiAl6V4 samples, Bioprinting 16 (2019) e00054, https://doi.org/10.1016/j.bprint.2019.e00054.
[60] X. Xu, H. Xu, Q. Chai, Z. Li, Z. Man, W. Li, Novel functionalized Ti6Al4V scaffold for preventing infection and promoting rapid osseointegration, Mater. Des. 226 (2023) 111612, https://doi.org/10.1016/j.matdes.2023.111612.
[61] B.M. Hidalgo-Robatto, M. López-Álvarez, A.S. Azevedo, J. Dorado, J. Serra, N. F. Azevedo, P. González, Pulsed laser deposition of copper and zinc doped hydroxyapatite coatings for biomedical applications, Surf. Coating. Technol. 333 (2018) 168–177, https://doi.org/10.1016/j.surfcoat.2017.11.006.
[62] C. Yuan, Y. Miao, Y. Chai, X. Zhang, X. Dong, Y. Zhao, Highly water-stable zinc based metal–organic framework: antibacterial, photocatalytic degradation and photoelectric responses, Molecules 28 (18) (2023) 6662, https://doi.org/10.3390/molecules28186662.
[63] Y. Shi, Z. Xue, P. Li, S. Yang, D. Zhang, S. Zhou, Z. Guan, Y. Li, L.N. Wang, Surface modification on biodegradable zinc alloys, J. Mater. Res. Technol. (2023), https://doi.org/10.1016/j.jmrt.2023.06.149.